Celestial Mechanics and Estimating the Termination of the Holocene Warm Period

Correspondence to
johnparmentola@gmail.com

Vol. 3.1 (2023)
pp. 9-32

John A. Parmentola

The RAND Corporation, Santa Monica, CA 90401 USA

Abstract

This paper addresses several issues concerning Milankovitch Theory and its relationship to paleoclimate data over the last 800,000 years. The approach taken treats the insolation as it is physically, a time-dependent wave. A parameter free model, based solely on the earth's celestial motions and the sun's rays, is presented that partitions the precession index (the precession modulated by the eccentricity) wave and the obliquity wave contributions to the percentage change between successive mean-daily-insolation minima and maxima at 65N latitude during the summer solstice. The model predictions indicate that the precession index contribution dominates such insolation changes and correlates with the occurrences of interglacial and glacial periods and temperature trends over the last 800,000 years. The predictions also indicate that all interglacial terminations over this period occur in the same manner through synchronized constructive interference of the precession index and obliquity waves. Similarly, all interglacial inceptions coincide with synchronized constructive interference of the precession index and obliquity waves, except for the timing of two inceptions, Marine Isotope Stage (MIS) 18d and 13c. These specific timing discrepancies are associated with deep ice cores, which have also been noted by Parrenin et al. through a comparison of Lisiecki and Raymo benthic δ^{18}O and EPICA Dome C (EDC) ice core datasets. Finally, the model enables the classification of interglacial periods into two distinct types based on wave interference that approximately accounts for their different durations. This classification strongly suggests that the current warm period, MIS 1, is very similar to MIS 19c that occurred about 787,000 years ago. When extended into the future, the repetitive wave pattern deduced from the model also enables an estimate for the Holocene warm period termination of 500 years from present.

Keywords: Milanovich cycles; insolation wave; daily-insolation minima and maxima, glacial and interglacial periods; temperature trends last 800 000 years; model predictions.

Submitted: 27-12-2022, Accepted 01-02-2023. https://doi.org/10.53234/SCC202301/11

1. Introduction

Since Milutin Milankovitch's seminal papers (Milankovitch, 1998) concerning the occurrence of ice ages, numerous papers have supported (Hays et al., 1976; Imbrie, 1982; Imbrie et al., 1986; Zachos et al., 2001; Gradstein et al., 2005; Huybers et al., 2011; Roe, 2006) and challenged (Wunsch, 2004; Berger, 2012) his hypothesis that changes in insolation at northern latitudes during the summer solstice is the likely cause of ice sheet changes associated with ice age occurrences. In its most basic form, Milankovitch Theory is a set of insolation conditions on the earth's climate system that have been shown to correlate with features in paleoclimate data.

A substantial number of papers have connected eccentricity, precession, and obliquity cyclical behaviors to features in the paleoclimate data (Lisiecki et al., 2005; Lisiecki, 2010). For example, these celestial parameters, as well as the insolation, exhibit specific characteristic frequencies that are also found in spectral analyses of paleoclimate data over the Pleistocene (Meyers et al., 2008). However, this approach does not completely account for interglacial and glacial durations and the timing of the prominent temperature excursions in paleoclimate data, such as those exhibited in EDC ice core data and other datasets (NCEI, 2007; Jouzel, 2013).

In this paper, the insolation is described physically as a time-dependent wave. It is analogous to an AM radio wave. Its wave-like nature is produced by the "beating" of the earth's celestial motions on the solar irradiance (about 1,368 W/m^2) resulting in its complex time-dependent distribution over the earth's surface. Each of the three celestial motions, precession, eccentricity, and obliquity, contributes a wave component to the insolation. Like ordinary waves, they can produce a beat-like structure through constructive and destructive interference. This description begs several questions. How large in magnitude is each of these wave components, and how do they interfere? Does the interference manifest itself in the paleoclimate data, and if so, how? Does the description of the insolation as a wave and its components have any predictive power for determining the reoccurrence and duration of interglacial and glacial periods? The objective of this paper is to answer these questions.

The results presented are described in temporal space as opposed to typical frequency space analyses for two reasons. First, paleoclimate data is commonly represented as a time series. The goal of this paper is to present a model that accounts for the features in the data as a function of time. Second, the three basic celestial parameters, the precession, eccentricity, and obliquity, are all quasiperiodic functions of time. They have no fixed period as can be seen from the following graphs of their half-cycles,

F*igure 1: Precession half-cycle durations during the period -843,900 years to +54,200 (IMCCE, 2018).*

for the precession, and

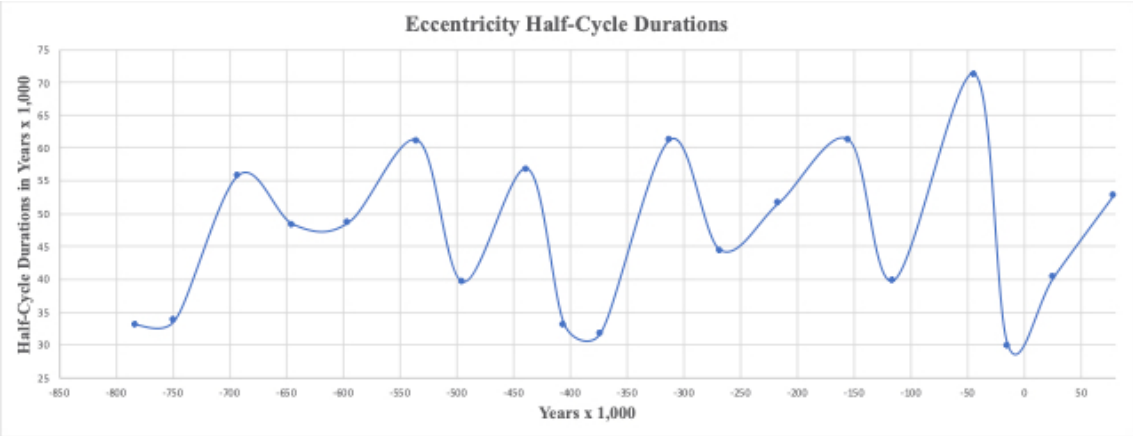

Figure 2: Eccentricity half-cycle durations during the period -815,000 to +79,000 years (IMCCE, 2018).

for the eccentricity, and

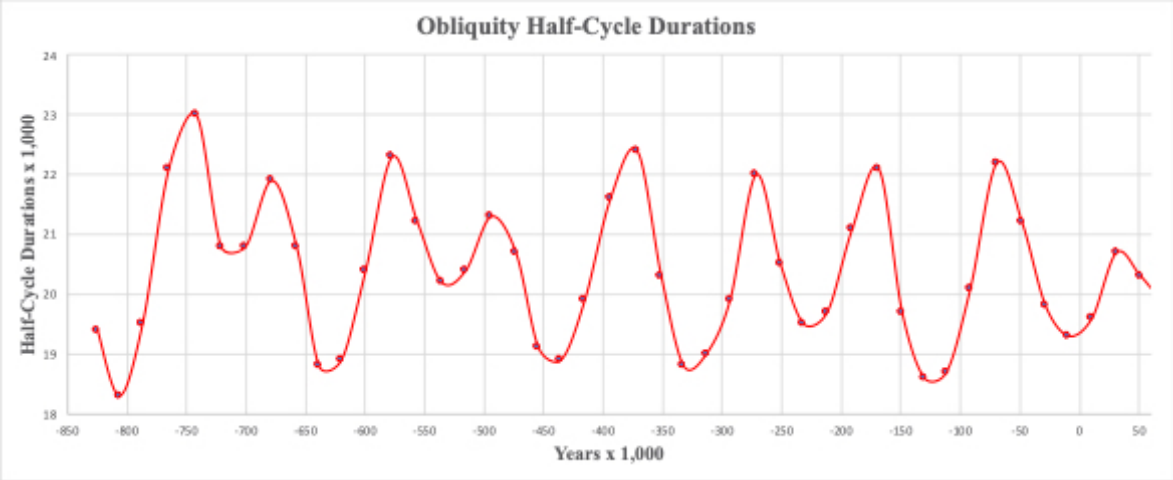

Figure 3: Obliquity half-cycle durations during the period -844,700 years to +51,100 years (IMCCE, 2018).

for the obliquity.

The shortest cycle of the three celestial parameters is that of the precession, which, over the last 800,000 years, on average, has been about 21,000 years. That of the obliquity has been about 41,000 years and the eccentricity about 94,000 years. However, the variation in these cycles and their half-cycles is quite large. For example, precession half-cycles vary from 7,000 to 15,000 years, the obliquity half-cycles from 18,000 to 23,000 years, and the eccentricity half-cycles from 30,000 to 70,000 years. In terms of timescales, the precession sets the scale for the time-dependent behavior of the insolation. As will be demonstrated through a time series comparison, the quasiperiodic nature of these parameters plays an essential role in the timing of wave interferences and prominent features in the paleoclimate data.

In terms of physical effects, the obliquity primarily affects the angular distribution of the insolation over the earth. In a half-cycle, it shifts the sun's rays south to north and vice versa by about 2.4 degrees in latitude or roughly 267 km. This shift changes the angle the sun's rays make with the vertical at

each illuminated point on the earth's surface resulting in a comparatively small overall effect on the insolation amplitude.

The most significant effect on the insolation amplitude comes from the combination of the precession and eccentricity, the precession index (sometimes referred to as the climate precession.) It is defined as the precession modulated by the eccentricity and physically accounts for insolation minima and maxima. For example, when the earth is at perihelion (the closest distance to the sun), and the earth's axis points toward the sun, the insolation approaches a maximum for the northern hemisphere. Fast forward about 11,000 years, an average precession half-cycle, the earth's axis points toward the sun at aphelion (the farthest distance from the sun) the insolation approaches a minimum for the northern hemisphere. The change from maximum to minimum and vice versa can be quite significant (more than 100 W/m^2) at northern latitudes during the summer solstice and is driven by changes in the eccentricity over a precession half-cycle. This qualitative analysis suggests that the insolation can be approximated by the effects produced by just two parameters, the precession index, and the obliquity at insolation maxima and minima.

Over the last 800,000 years, the insolation has transitioned from maxima to minima and vice versa a total of 74 times. These transitions range in percentage from about +28% to -19% with half-cycle durations (the average is about 11,000 years) that range from 4,200 to 16,900 years. They are represented by mean daily insolation predictions at 65 degrees north latitude during June in Figure 4.

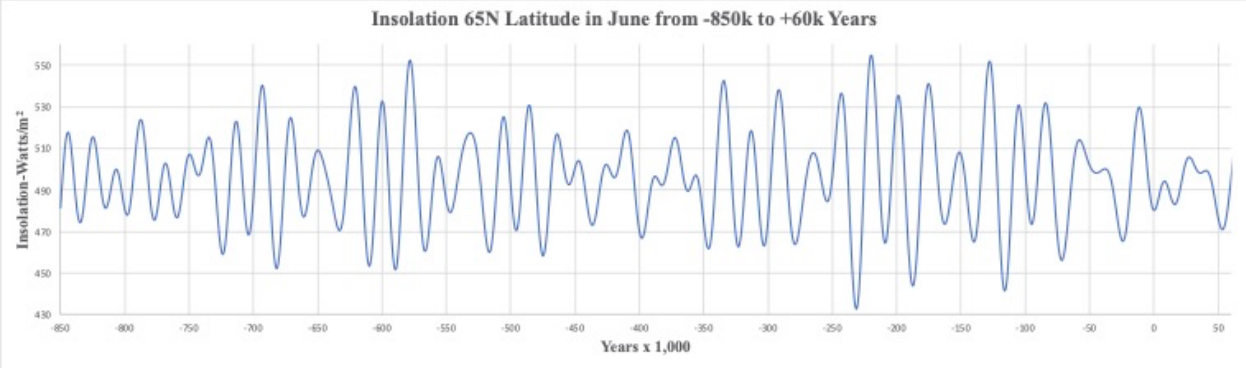

Figure 4. Mean-daily-insolation at 65N latitude in June for the period -850,000 to +60,000 years (IMCCE, 2018).

However, the number of prominent temperature excursions indicated in paleoclimate data is at best 13, which is represented by EPICA Dome C ice core data from Antarctica in Figure 5. This graph is a temperature reconstruction from ice core data using deuterium as a proxy; however, it is model dependent. There are physical effects that can affect the dating of temperature changes inferred from ice cores, which are discussed further in Section 3 where model predictions are compared with paleoclimate time series data.

Reconciling the 74 transitions of Figure 4 in terms of timing and amplitude with the prominent temperature excursions in Figure 5 is a formidable theoretical challenge. These features are affected by eccentricity, precession, and obliquity cyclical behaviors, which have been computed from -250 million to +250 million years (IMCCE, 2018; Laskar et al., 2004). According to the Milankovitch hypothesis, their determination provides a consistent temporal calibration that should correlate insolation changes with features in the paleoclimate data.

Figure 5 indicates that steep rises and subsequent major temperature declines are comparatively infrequent; however, the timescale of these changes is roughly 10,000 years, which approximately

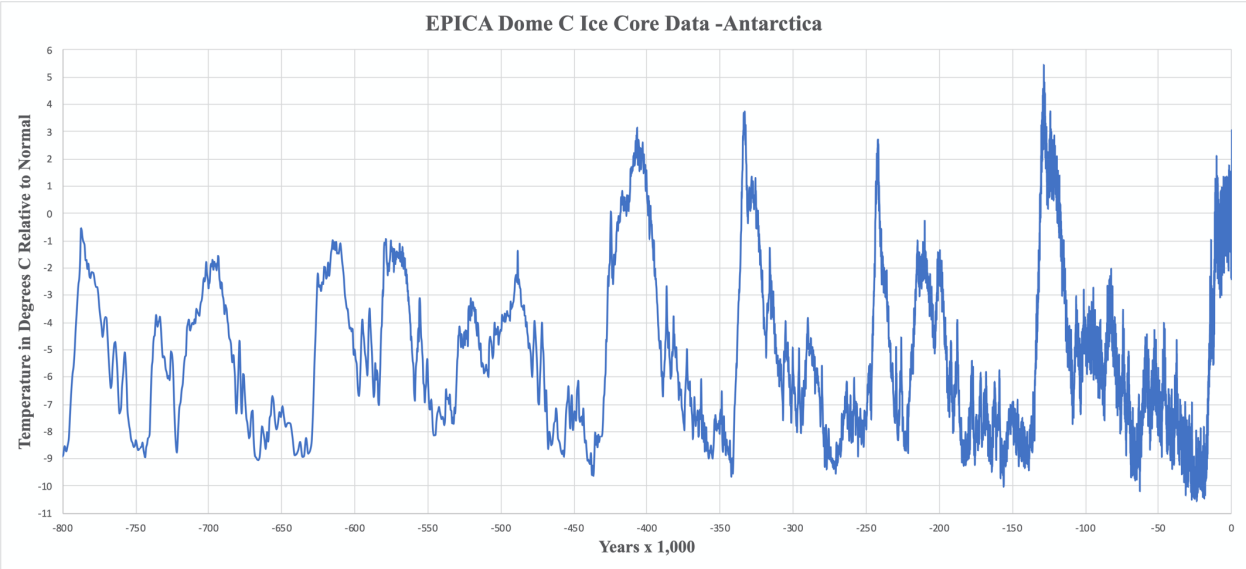

Figure 5. EDC ice core data based on a temperature reconstruction model using deuterium as a proxy presented in degrees centigrade relative to normal from -800,000 years to the present (NCEI, 2007).

coincides with the average precession half-cycle. What, if any, relationship is there between insolation changes and prominent features in the paleoclimate data? Are there specific insolation changes that are special, or are there trends in the insolation over time that correlate with significant changes in the paleoclimate data? To gain some insight into correlations, one might consider the largest changes in insolation from successive minima to maxima, and vice versa to see if these influenced the paleoclimate data more than other insolation changes. Such an approach would also capture insolation trends (as opposed to just individual changes) that could explain certain reoccurring features in the paleoclimate data over time.

Since the obliquity primarily affects the angular distribution of the solar irradiance over the earth's surface with a comparatively small effect on its amplitude over long cycles and the precession index is the primary driver of the insolation amplitude over shorter cycles, the product of the two contributions, the partition model, should well approximate the insolation at maxima and minima. This approximation separates these two effects over time and allows for their time series comparison with the paleoclimate data that implicitly includes the quasiperiodic nature of the three celestial parameters.

2. Methodology

The partition model presented below in Section 3 is not a climate model. There is no inclusion of any aspect of the earth's climate in the model. It is a parameter-free kinematic model based on the three celestial motions of the earth and the sun's rays. The model provides a set of points in time for the obliquity and precession index contributions that represent the percentage change between successive mean-daily-insolation extrema at 65N in June. The model predictions for the insolation are compared with the corresponding theoretical calculations of J. Laskar et al. (IMCCE, 2018; Laskar et al., 2004) showing excellent agreement. An interpolation is made between the set of points for the obliquity and precession index contributions that enables a wave description of these separate contributions to the insolation. In Section 4, the interpolated predictions are compared with the EDC ice core dataset and interpreted using waves and their interference. In Section 5, an estimate for the Holocene warm period termination is presented. Section 6 summarizes the principal results.

3. The Partition Model

This paper assumes the percentage change between successive mean-daily-insolation maxima and minima at 65 degrees northern (65N) latitude during the summer solstice (June) over the last 800,000 years, substantially influenced the prominent features in paleoclimate data such as the EDC dataset depicted in Figure 5.

The main point of this paper is to provide insight into the insolation's time-dependent wave behavior through its separation into precession index and obliquity contributions. Both quasiperiodic behaviors are shown to correlate with the prominent features in paleoclimate data over the last 800,000 years in Section 3.

The separation is accomplished, in part, through an application of the computational tool developed by J. Laskar et al. (IMCCE, 2018; Laskar et al., 2004). The eccentricity, precession, obliquity, and insolation parameters are specified at a time with a temporal resolution of 100 years using Laskar's tool. There are no free parameters in the model.

The insolation, Q, is assumed to be of the form,

$$Q = A \cdot B, \tag{1}$$

where A and B are respectively the precession index and obliquity contributions to the insolation. In Appendix A, B is shown to depend on latitude and the sun's declination angle. Because daylight hours depend on latitude and the sun's declination angle, the mean-daily-insolation, $\overline{Q}$, is dependent on the mean-daily-obliquity contribution, $\overline{B}$. By averaging equation (1) over daylight hours, the mean-daily-insolation is given by

$$\overline{Q} = A \cdot \overline{B} \tag{2}$$

It is straightforward to show from equation (2) that a fractional change in $\overline{Q}$ produced through changes in A and $\overline{B}$ is approximately given by the sum of the fractional contributions,

$$\frac{\Delta\overline{Q}}{\overline{Q}_i} \cong \frac{\Delta A}{A_i} + \frac{\Delta\overline{B}}{\overline{B}_i}, \tag{3}$$

where $\frac{\Delta A}{A_i}$ and $\frac{\Delta\overline{B}}{\overline{B}_i}$ are respectively the fractional precession index and obliquity contributions to the fractional change in the mean-daily-insolation, $\frac{\Delta\overline{Q}}{\overline{Q}_i}$, with $\Delta\overline{Q} = \overline{Q}_f - \overline{Q}_i$, $\Delta A = A_f - A_i$, and $\Delta\overline{B} = \overline{B}_f - \overline{B}_i$ are the respective changes in the mean-daily-insolation, and the precession index and obliquity contributions to the mean-daily-insolation with the subscripts, i and f, designating the initial and final states. The correction cross-term, $\frac{\Delta A}{A_i} \cdot \frac{\Delta\overline{B}}{\overline{B}_i}$, to equation (3) will be shown to be negligible.

The approximation represented by equation (3) implies that the precession index and obliquity contributions to the mean daily insolation simply add. As will be demonstrated in Section 3.3, this translates into the superposition of a precession index wave and an obliquity wave. This separation also enables each of these waves to be compared with EDC data as a time series.

3.1 Precession Index Contribution

The earth's eccentricity has varied by more than an order of magnitude from about 0.004 to 0.05 during the last 800,000 years. The key to understanding the eccentricity's effect on the insolation at northern latitudes during the summer solstice is its change from the time the earth's axis points toward the sun at perihelion to the time it points toward the sun at aphelion. While the timescale of the precession index contribution to the insolation is affected by the eccentricity, its short-term half-cycle is primarily due to the precession.

The comparatively small eccentricity changes over these precession half-cycles enable the approximate determination of the precession index contribution to the fractional change between mean-daily-insolation extrema. As discussed further below, the precession index contribution to the percentage change between successive insolation extrema at 65N during June takes the form of a quasiperiodic wave; however, its half-cycle durations differ from those of the precession.

Assuming the insolation depends on the inverse distance squared from the sun multiplied by an overall constant, the fractional change of the precession index contribution during a perihelion to aphelion half-cycle transition is given by

$$\frac{\Delta A_{p\to a}}{A_p} = \frac{(1-e_p)^2}{(1+e_a)^2} - 1, \tag{4}$$

where the perihelion subscript, p, and aphelion subscript, a, are the initial and final states, respectively. Equation (4) is well approximated by

$$\frac{\Delta A_{p\to a}}{A_a} \approx -2\left(e_a + e_p\right) + e_p^2 + 4e_a e_p + 3e_a^2\,, \tag{5}$$

where the linear term dominates. Similarly, in transitioning from aphelion to perihelion, the corresponding fractional precession index contribution is given by

$$\frac{\Delta A_{a\to p}}{A_a} = \frac{(1+e_a)^2}{(1-e_p)^2} - 1, \tag{6}$$

which is also well approximated by

$$\frac{\Delta A_{a\to p}}{A_a} \approx 2\left(e_a + e_p\right) + e_a^2 + 4e_a e_p + 3e_p^2, \tag{7}$$

where again the first term dominates, and the subscripts have corresponding interpretations. The eccentricity, e, depends on time and is specified by Laskar's tool at the time of each mean-daily-insolation maximum and minimum during June at 65N latitude.

In deriving equations (4) and (6), the earth-sun distances at perihelion, $R_p = a\cdot\left(1-e_p\right)$, and aphelion, $R_a = a\cdot(1+e_a)$, are used, where, a, is the semi-major axis of the earth's orbit. The semi-major axis is assumed constant during an insolation transition between successive extrema, which implies eccentricity changes result from changes in the semi-minor axis. Also, because the

eccentricity is a slowly varying function of time, differences in the time specification of insolation extrema and when the earth's axis successively points toward the sun at perihelion and aphelion and vice versa have a comparatively small impact on the insolation. An error analysis that supports this conclusion is presented in the next subsection.

3.2 Obliquity Contribution

The comparatively small and gradual change in the earth's tilt angle also enables the approximate determination of the obliquity contribution to the fractional change between successive mean-daily-insolation extrema. By specializing to the summer solstice (the sun's declination angle equals the obliquity angle), in Appendix A, the fractional obliquity contribution to successive mean daily insolation during June is shown to be of the form,

$$\frac{\Delta\overline{B}}{\overline{B}_i} = \frac{h_f \cdot \sin\emptyset \cdot \sin\theta_f + \cos\emptyset \cdot \cos\theta_f \cdot \sin h_f}{h_i \cdot \sin\emptyset \cdot \sin\theta_i + \cos\emptyset \cdot \cos\theta_i \cdot \sin h_i} - 1, \tag{8}$$

where $\emptyset$ is the latitude $= 1.134$ radians or $65N$, and θ_i and θ_f are the initial and final obliquity angles specified in radians with h_i and h_f the initial and final hour angles determined by,

$$h_j = \cos^{-1}\left(-\tan\emptyset \cdot \tan\theta_j\right), \tag{9}$$

which is also in radians. The obliquity range, $0.386 \leq \theta \leq 0.428$ radians, implies a maximum percentage obliquity contribution to successive mean-daily-insolation extrema during June at 65N latitude is about 8.6% from equations (8) and (9); however, this maximum is never realized (see further discussion below). The obliquity angle, θ, is specified by Laskar's tool at the time of each mean-daily-insolation maximum and minimum at 65N latitude during June. For successive insolation extrema transitions, equations (8) and (9) are surprisingly well approximated by

$$\frac{\Delta\overline{B}}{\overline{B}_i} \approx 2 \cdot \left(\theta_f - \theta_i\right). \tag{10}$$

The linear terms in equations (5), (7), and (10) can be used to provide reasonable "back of the envelope" estimates for the fractional change between successive mean-daily-insolation extrema at 65N latitude during June.

3.3 The Wave Description

The more accurate partition model predictions are utilized by substituting equations (4), (6), (8), and (9) into equation (3) to compare the model predictions with the corresponding Laskar predictions. This comparison is shown in Figure 6.

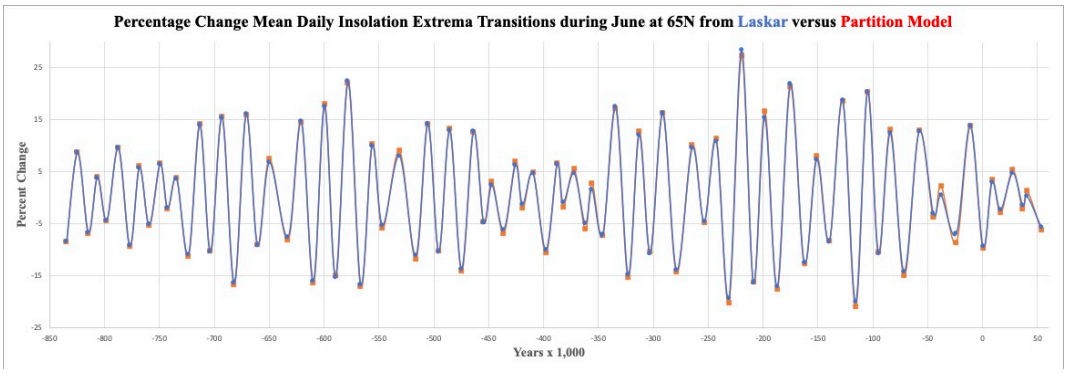

Figure 6. Comparison of the partition model approximation to the percentage change between successive mean-daily-insolation extrema at 65N latitude in June with the predictions of J. Laskar et al. in Figure 3.

The blue dots follow from Laskar's tool, and the red dots are partition model estimates for the percentage change between successive mean-daily-insolation extrema at 65N latitude during June. A point wise error analysis of Figure 6 is represented in Figure 7,

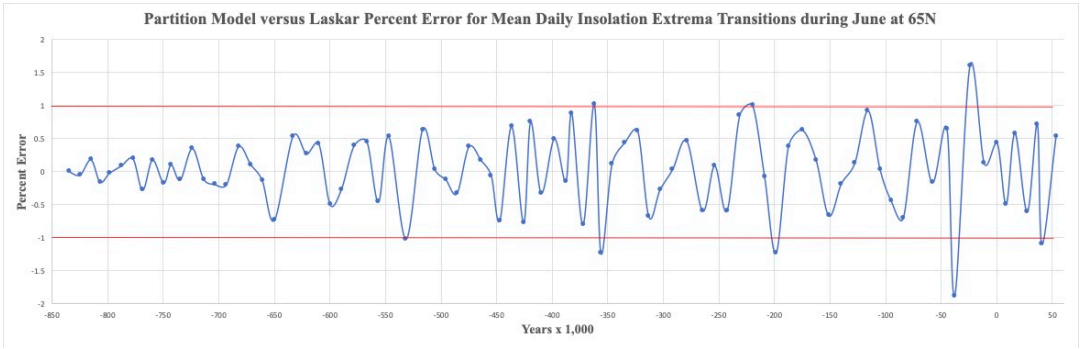

Figure 7. An analysis of Figure 7 indicates a + or -1% error bound on most points (horizontal red lines) with several points between + or -1 and + or -2%.

For most points, the error is bounded by + or -1%. The comparatively few exceptions are of no consequence to the analysis presented below.

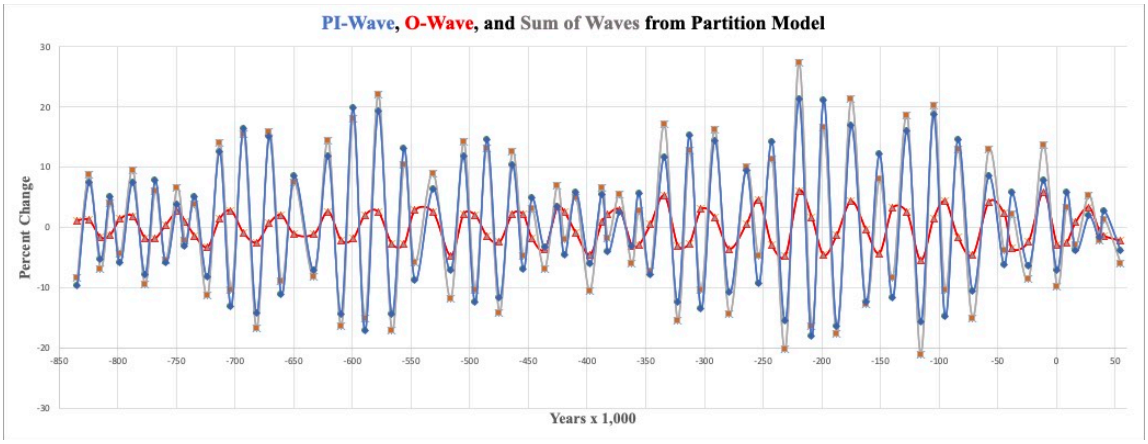

Figure 8. Partition model estimates for the precession index wave (blue curve), obliquity wave (red curve), and their sum (grey curve with red dots) associated with the percentage change between successive mean- -daily-insolation maxima and minima at 65N latitude during June from -844,200 to +53,500 years (IMCCE, 2018).

The complex "beat structure" in Figure 6 results from the superposition of the precession index and obliquity wave contributions to the percentage change between successive mean-daily- insolation extrema, which follow from equations (3), (4), (6), (8), and (9) and are represented in Figure 8.

The values greater or less than zero represent increasing or decreasing changes from each contribution to successive mean-daily-insolation extrema transitions. They, therefore, provide systematic trends associated with mean daily insolation changes over time, which are not evident in Figures 4 and 6. These increasing and decreasing trends will be shown to correlate with the prominent features in paleoclimate data.

Note that the precession index and obliquity contributions to successive mean-daily-insolation extrema from equations (4), (6), (8), and (9) contribute to the neglected cross-term corrections to equation (3). At best, these corrections are an order of magnitude less than the leading terms, which validates equation (3).

The three curves in Figure 8 are based on best fits to a sparse set of points. Nevertheless, the curves provide quantitative estimates, and qualitative behaviors as well as a conceptual language involving waves that will be exploited below to physically describe the prominent features of the EDC ice core data of Figure 5.

The obliquity contribution (red curve) in Figure 8 will be referred to as the O-Wave. It appears as a quasiperiodic wave of varying half-cycle duration having a narrowly bound amplitude. Its contributions range from about 6% (-219,600 years) to -5% (-115,700 years).

The precession index contribution (blue curve) will be referred to as the PI-Wave of recurring wave packets comprised of a precession carrier wave modulated by an eccentricity wave. It is contribution ranges from about 21% (-219,600 years) to -18% (-208,700 years). Note that the eccentricity primarily amplifies and reduces the insolation in a quasiperiodic manner through recurring PI wave packets.

The grey curve is the sum of the O-Wave and PI-Wave contributions. In terms of magnitude, the PI-Wave contribution to the insolation dominates the O-Wave. As will be demonstrated in the next section, the insolation trends represented by the PI-Wave approximately correlate with the prominent features of the EDC data. These aspects of the PI-Wave contradict the original Milankovitch Theory hypothesis (Milankovitch, 1998), which emphasizes the role of the obliquity in the occurrence of ice ages.

4. Time Series Comparison of the Model Predictions and EDC data

Because of the earth's highly complex climate system and unknown conditions in the past, its response to external effects such as celestial mechanical forcing is very challenging to predict. Adding to this complexity are internal effects within the earth system that can also affect its climate, such as volcanic eruptions, albedo changes, etc. Hence, the detailed behavior of the earth's climate between and during interglacial periods is far beyond the scope of this paper. Nevertheless, the predictions from the partition model will be used to interpret the EDC data. This semi-quantitative approach indicates that there are correlations between celestial mechanical forcing and prominent features in the data.

The comparison of EDC data modified by Marine Isotope Stage (MIS) designations (Berger et al., 2015) with the PI-Wave of Figure 8 is represented in Figure 9.

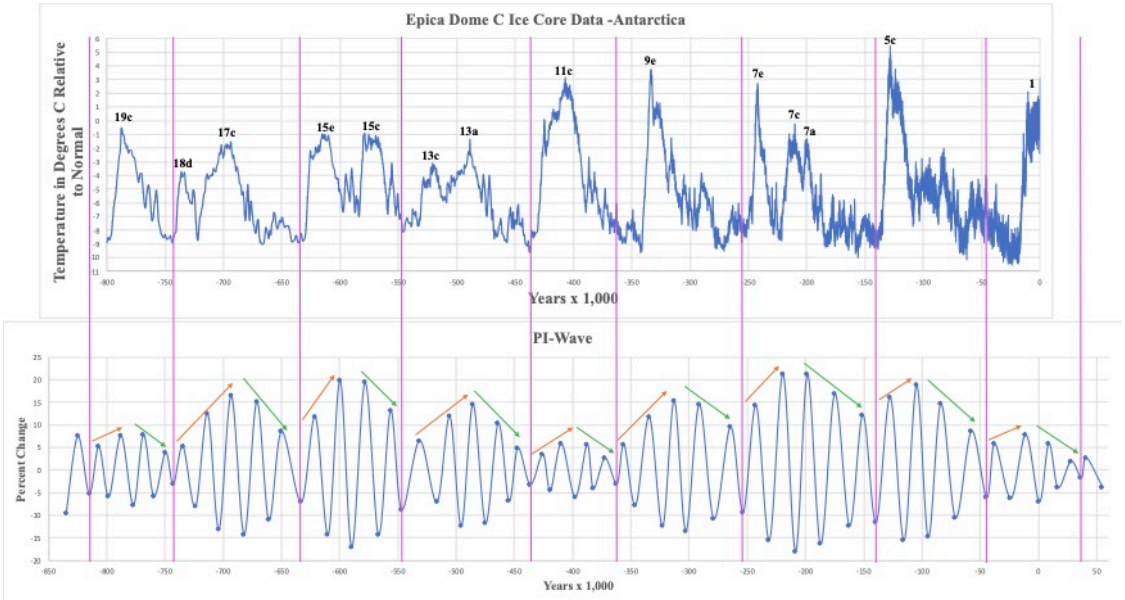

Figure 9. PI recurring wave packets (judiciously defined by purple vertical lines) approximately correlate with interglacial and glacial periods over the last 800,000 years. Precession carrier wave maxima trends qualitatively correlate with increasing temperature trends (red arrows) and decreasing maxima trends (green arrows) with decreasing temperature.

Visually, the quasiperiodic PI wave packets, which are specified by the vertical purple lines, roughly correlate with recurring interglacial and glacial periods. To determine occurrences of interglacial and glacial periods, simply follow the recurring PI wave packets. However, the relationship between the timing of prominent temperature excursions and the partition model predictions also depends on the O-Wave contributions (see further discussion below). Nevertheless, increasing temperatures in the EDC data coincide with increasing precession carrier wave maxima (red arrows), while declining temperature trends follow the decreasing trend in precession carrier wave maxima (green arrows). These amplitude trends are primarily due to eccentricity changes. The eccentricity during precession carrier wave cycles amplifies and reduces the insolation over substantial periods, which roughly correlate with the inception and termination of interglacial periods.

Note that some temperature trends are interrupted by precession carrier wave amplitude reductions that appear to "split" the temperature peaks into MIS pairs, namely, 18d-17c, 15e-15c, 13c-13a, 7e-7c, and 7c-7a (see further discussion below). Also, note the similarity in Figure 9 between the wave packet to the far left (associated with MIS 19c) and the last one to the far right (associated with MIS 1), which is the Holocene, but more about this relationship in the next section.

The O-Wave contribution to the percentage change of successive mean-daily-insolation extrema at 65N during June also qualitatively correlates with EDC temperature excursions as indicated in Figure 10. The comparison in Figure 10 indicates that both data sets have similar quasiperiodic behaviors with the O-Wave systematically lagging the EDC data (see discussion below). It also indicates that there were 20 O-Wave maxima and 13 prominent temperature excursions with numerous temperature "bumps" in between over the last 800,000 years. Also note that from -430,000 years to the present, the obliquity wave maxima tend to be higher, and the minima lower than the period -800,000 to -430,000 years. This behavior may, in part, account for the systematically higher and lower

temperatures during the period -430,000 years to present compared to the earlier period often referred to as the mid-Brunhes Climate Transition.

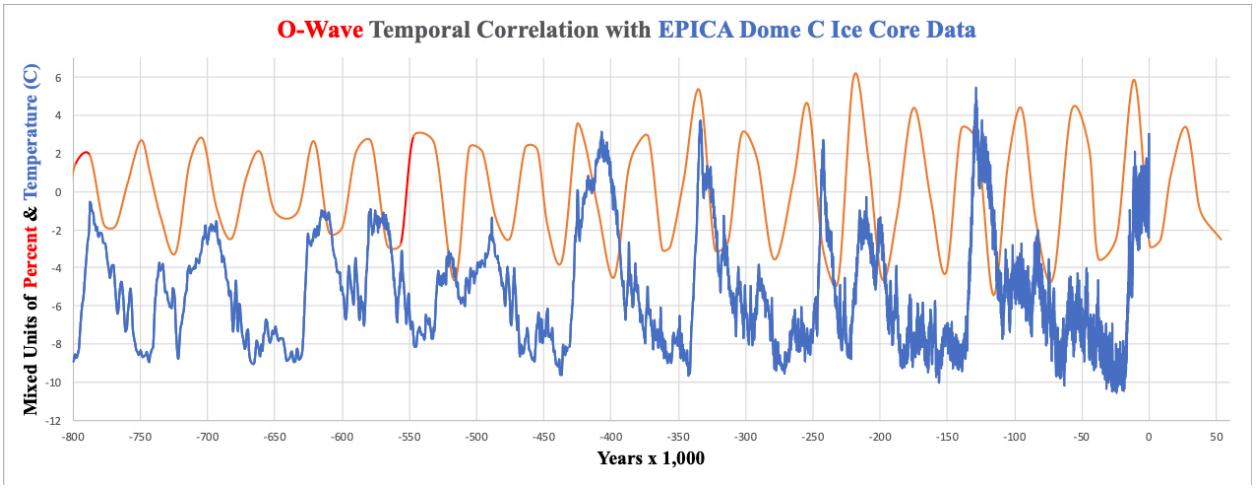

Figure 10. O-Wave predictions from the partition model and EDC data indicate a qualitative temporal correlation between O-Wave maxima and EDC temperature peaks. The O-Wave curve is constructed from 85 data points while the EDC data involves 5,788 points.

The temporal correlation between the O-Wave oscillations and EDC temperature excursions can be improved by shifting O-Wave data by +10,000 years as indicated in Figure 11.

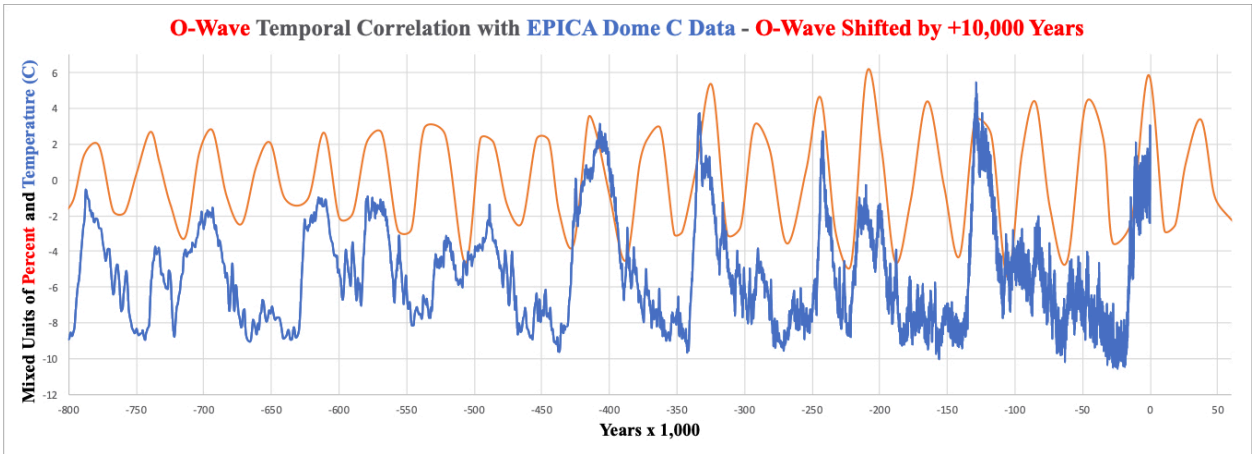

Figure 11. O-Wave predictions from partition model and EDC data with the O-Wave temporally shifted by +10,000 years indicating an improved qualitative correlation between O-Wave maxima and EDC temperature peaks.

Note, the 10,000-year shift is comparable to the average precession carrier wave half-cycle duration. The timing differences between the O-Wave contribution and the temperature excursions are ameliorated through interference between the PI- and O-Wave.

Utilizing the above wave taxonomy, interglacial periods can be classified into two types. Those of Type I occur over one precession carrier wave cycle. During such a cycle, there is an approximate constructive interference between the precession carrier and O waves. Those of Type II occur over two precession carrier cycles; however, there is constructive and destructive interference between the precession carrier and O waves during such cycles.

Using MIS designations, those of Type I are 19c, 15e, 15c,13c, 9e, 7e, 5e, and 1, which are represented in Figure 12.

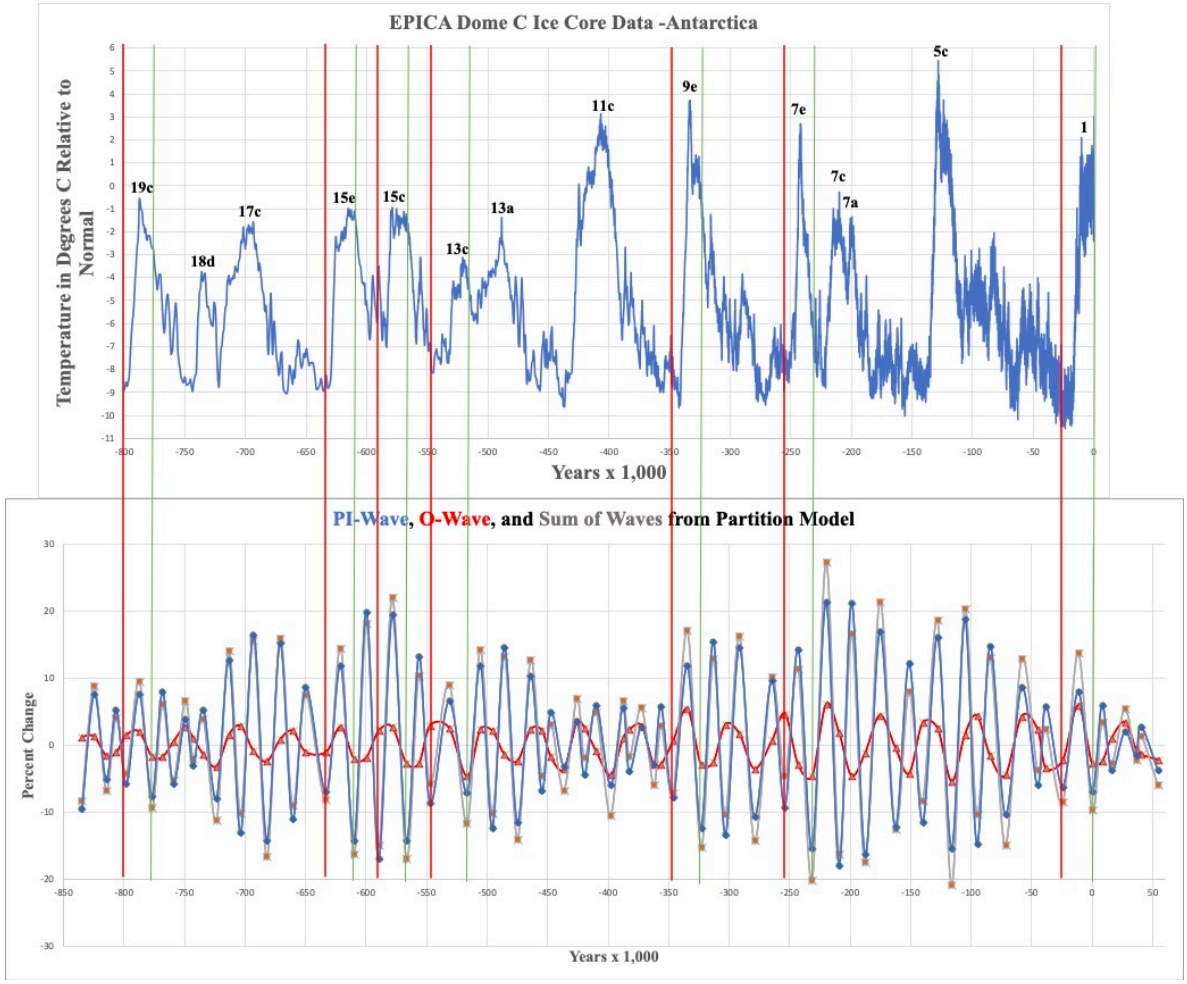

Figure 12. Type I interglacial initiations (red vertical lines) are followed by interglacial terminations (green vertical lines). Initiations coincide with concurrent PI-Wave, and O-Wave increases to the right of the red vertical lines, and terminations coincide with corresponding concurrent declines ending in green vertical lines.

Each pair of vertical red and green lines extending across both graphs relates the duration of each precession carrier cycle and its corresponding MIS interglacial. For Type I, all PI-Wave contributions constructively interfere with O-Wave contributions except for MIS 7e (see further discussion below). Starting from the right of each vertical red line, both contributions concurrently increase to approximately synchronized maxima associated with the red dots of the grey curve and then decline concurrently to the vertical green lines terminating on the red dots of gray curve minima. The vertical green lines define all interglacial terminations, which are comparatively sharp. Note the role of the O-Wave is to enhance (constructive interference) the precession carrier wave maxima and minima as indicated by the red dots associated with grey curve maxima (excluding for MIS 7e) and minima (including MIS 7e). The termination of MIS 1, the Holocene, will be discussed in the next section.

For MIS 7e, the PI- and O-Wave contributions are initially out of phase by about ¼ of an O-Wave cycle; however, they partially constructively interfere as the PI-Wave contribution increases to the right of the indicated vertical red line. The duration of this interglacial is likely cut short because the O-Wave contribution subsequently destructively interferes with the PI-Wave contribution. However,

MIS 7e terminates like all others of Type I as indicated by the deep minimum at the green line (the grey curve red dot minimum).

Note also, the delay in the initiation of interglacial MIS 13c, which has the longest precession carrier wave cyclical duration of about 30,000 years. Its precession carrier wave maximum represents a decline from the earlier maximum in Figure 12. Note the O-wave contribution is out of synchronization, which broadens the insolation maximum. Also, the amplification rate of the insolation during this period is comparatively low due to its long duration. This delay is described further below, along with another initiation delay associated with a Type II interglacial.

The interglacial periods of Type II are MIS 18d, 17c, 13a, 11c, and 7c-7a. The latter hyphenated designation is further explained below. Each of these periods involves a pair of precession carrier wave maxima trending higher, as depicted in Figure 13.

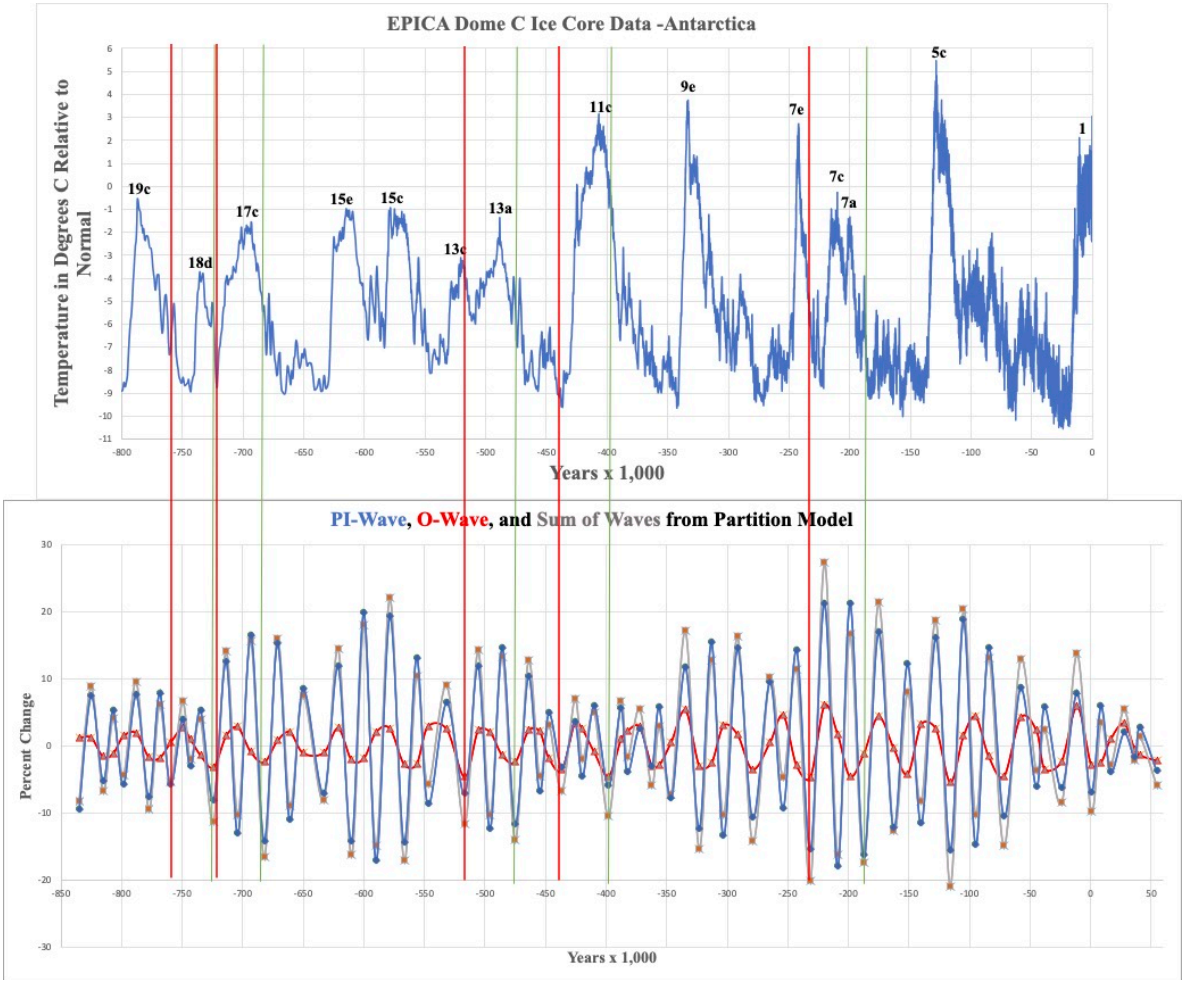

Figure 13. Type II interglacial initiations (red vertical lines) are followed by interglacial terminations (green vertical lines). Initiations coincide with concurrent PI-Wave and O-Wave increases to the right of the red vertical lines, while terminations coincide with in phase PI-Wave and O-Wave minima that coincide with corresponding green vertical lines. Note that the pair of green and red lines associated with the MIS 18d-17c split the interglacial.

Again, the pair of vertical red and green lines identify the temporal extent of two precession carrier wave maxima and minima and their corresponding interglacial period. The O-Wave contributions occur over a longer half-cycle than the Type I set. In all cases, an O-Wave maximum is approximately

in phase with the first precession carrier wave maximum (constructive interference). The O-Wave is then out of phase with the next precession carrier wave minimum and maximum (destructive interference). Eventually, the O-Wave contribution ends approximately in phase with the final precession carrier wave minimum except for MIS 7c-7a, which is about ¼ of an obliquity wave cycle out of phase (about 11,000 years). However, in the latter case, the O-Wave contribution is negative at the second precession carrier wave minimum, so it constructively contributes to the MIS 7a termination as indicated by the deep minimum at its green vertical line (red dot minimum of the grey curve).

MIS 7c-7a appears to be an interglacial that is split in two. It is associated with successive precession carrier wave maxima and minima that have the largest magnitudes over the last 800,000 years. There is a concurrent decline in the precession carrier wave and O-Wave contributions between the precession carrier wave peaks. The timing of this concurrent decline likely accounts for the split in the MIS 7c-7a interglacial. However, the MIS 7a temperature peak is of a very short duration, likely due to the destructive interference between the second precession carrier wave peak and the O-Wave. Note that MIS pairs 18d-17c, 15e-15c, 13c-13a, and 7e-7c also appear to be split by PI- and O-Wave cyclical behaviors.

All Type I and II interglacial durations are approximately determined by their precession carrier wave durations. However, there are delays in the initiation of MIS 18d (5,000–7,000 years) and MIS 13c (11,000–13,000 years). For MIS 18d, the precession carrier wave maximum to the right of the red line is a part of an insolation decline despite its enhancement from the O-Wave contribution (red dot on grey curve). The subsequent second precession carrier wave maximum (MIS 18d is of Type II) is even less by about 2%. This feature may account for the comparatively small MIS 18d temperature excursion. The relatively low rate of increasing insolation may also account for the comparatively small MIS 13c temperature excursion.

Both MIS 18d and 13c also represent deep ice cores (time is a function of core depth), where physical effects can affect the estimated time of these interglacial inceptions and terminations using ice core models. It has been noted (Parrenin et al., 2007) that the most significant timing discrepancies between paleoclimate datasets EDC and LR04 benthic $\delta^{18}O$ occur for MIS 18d and 13c. This comparison suggests that the partition model predictions for the timing of interglacial initiations and terminations could be correct and that another examination of the EDC data may resolve the timing discrepancies between the partition predictions presented here and the data.

Overall, the rates of insolation amplification and reduction as indicated by the recurring PI wave packets (enhanced by the obliquity contribution) appear to correlate with rising and declining EDC temperature excursions. And all interglacial terminations coincide with the same celestial mechanical forcing conditions.

5. Estimating the Holocene Warm Period Termination

To discuss the duration of interglacial terminations, a quantitative criterion is required that can be used across 800,000 years to define the interglacial termination period. For an interglacial, that criterion is the period from the PI-Wave maximum (second maximum for Type II) to the successive synchronized minimum.

The analysis presented above indicates that MIS 1 is a Type I interglacial. As such, it is expected to terminate because of PI- and O-Wave constructive interference. The MIS 1 one cycle classification

indicates that MIS 11c is an unlikely analog because it is Type II, which has been proposed in the literature (Berger et al., 2003; Rohling et al., 2010).
MIS 19c has also been identified as a possible Holocene analog based solely on the behavior of celestial parameters and comparable mean-daily-insolation changes (Vavrus et al., 2018). The analysis presented below addresses the similarities and differences between MIS 19c and MIS 1 based on PI- and O-Wave contributions to the percentage change between successive mean-daily-insolation extrema at 65N latitude during June.

As pointed out earlier in Figure 9, the O-Wave half-cycle durations of MIS 19c and MIS 1 are similar. They both are associated with an O-Wave cycle duration of about 37,000 years, with approximate half-cycles of 27,000 years on the upside and 10,000 years on the downside. They also have comparable declines in mean-daily-insolation from their maxima to minima. For MIS 19c, the decline is about 48 $W/m^{2,}$ while for MIS 1, it is about 50 W/m^2.

Their main difference is the estimated duration of their precession carrier wave cycle and half-cycle durations. For MIS 19c, the precession carrier wave cycle duration is about 21,000 years, while for MIS 1, it is about 24,000 years. This difference indicates that MIS 1 will likely be a longer interglacial than MIS 19c. In terms of interglacial terminations, the MIS 19c downside precession carrier wave half-cycle duration is about 10,500 years, while for MIS 1, it is about 11,600 years.

In Figures 12 and 13, Type I and II terminations end on grey curve red dot minima that involve O-Wave enhancements (constructive interference) to precession carrier wave minima. The following table summarizes the termination estimates for each MIS based on their downside precession carrier wave half-cycle duration.

Table I: MIS termination duration estimates based on the last precession carrier wave peak to the vertical green line in Figures 12 and 13.

Type I	MIS #	Termination (years)
	19c	10,500
	15e	11,100
	15a	11,700
	13c	14,800
	9c	11,400
	7e	11,500
	5e	11,800
	1	11,600
Type II	18d	10,800
	17c	11,100
	13a	10,800
	11c	11,800
	7c-7a	11,200

These termination estimates are all comparable (within hundreds of years of each other) in duration except for MIS 13c, which has the longest cyclical duration and the largest downside precession carrier wave half-cycle duration of 14,800 years.

Assuming the vertical green line for MIS 1 in Figure 12 is accurate, its termination will occur at 500 years from the present based on just celestial mechanical forcing. This estimate coincides with the local minimum in insolation using Laskar's tool as indicated in Figure 14.

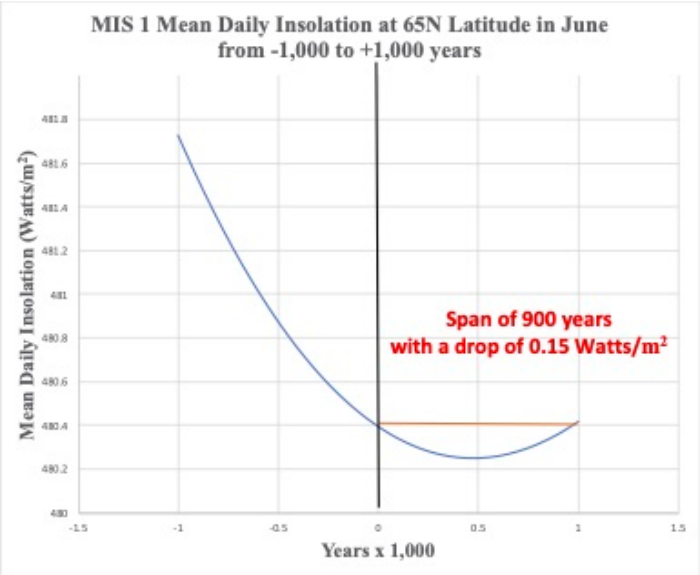

Figure 14. MIS 1 mean-daily- insolation at 65N latitude during Junefrom -1,000 to +1,000 years. The shallow minimum at +500 years measured from the vertical black line estimates the Holocenetermination, which coincides with the vertical green line in Figure 12.

It is hard to imagine, given other uncertainties, that an additional 0.15 W/m^2 decline of insolation from the present to 500 years in the future can make much of a difference regarding the termination of the current Holocene warm period. Given the very shallow minimum and the likelihood that the effects causing a temperature descent are cumulative, a more reasonable low-resolution estimate for the resolution estimate for the termination would be sometime within the next 500 years.

MIS 19c shares the same MIS 1 feature as indicated in Figure 15, which also has a relatively shallow minimum over 1,100 years. Note that all other interglacial terminations share this common feature.

Given the consistent recurrence of the interglacial terminations based on celestial mechanical forcing over the last 800,000 years, it is likely that there is a common physical climate mechanism that accounts for interglacial terminations. Milankovitch Theory focuses on northern latitudes at or greater than 65N because of the potential for ice sheet growth due to the decline in mean-daily-insolation at these latitudes during June over thousands of years. The substantial reduction in the mean-daily-insolation over the last 11,100 years for the Holocene has likely had a cooling effect on the air over a range of latitudes. This latitudinal range is due to a tradeoff between increasing insolation as the latitude decreases (the obliquity has decreased over the last 11,100 years) along with a concurrent decline in daylight hours. As examples, Figures 16 and 17 demonstrate the extensive nature of this latitudinal effect for MIS 19c and 1,

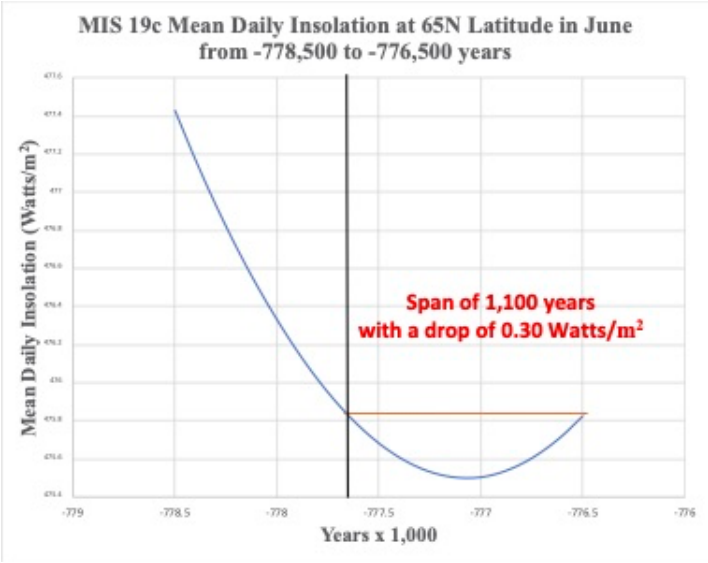

Figure 15. MIS 19c mean-daily-insolation at 65N latitude during June from -778,500 to -776,500 years. The shallow minimum at 600 years measured from the vertical black line is a termination estimate that coincides with the vertical green line in Figure 12

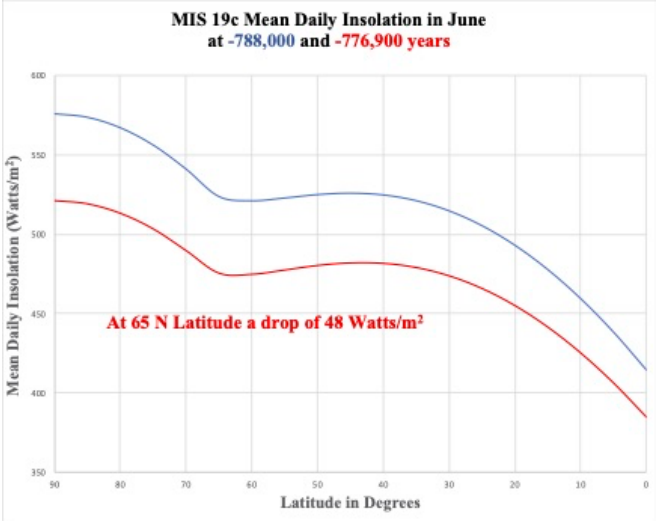

Figure 16. Latitudinal effect on mean-daily-insolation over a period of 11,100 years for MIS 19c (IMCCE, 2018).

This gradual reduction in mean-daily-insolation during June over the last 11,100 years enables air at northern latitudes to more readily cool during the winter solstice (the hour angle significantly decreases), which has the potential to increase the dense cold air volume at northern latitudes. Similar insolation reductions have occurred many times over the last 800,000 years; however, the specific physical mechanism within the earth's climate system that couples to such insolation reductions to cause a temperature descent into a glacial remains uncertain. It is therefore impossible to predict the consequences of this insolation condition on the earth's climate in detail because of our poor understanding of the earth's climate. The best that can be expected is relying on the recurring pattern described in this paper.

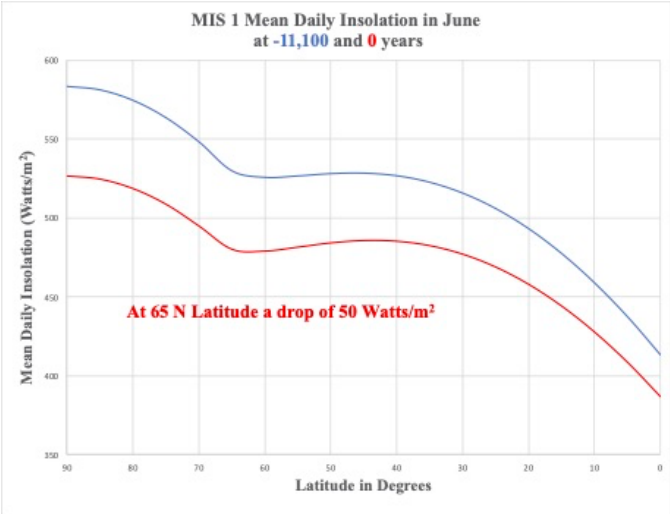

Figure 17. Latitudinal effect on mean-daily-insolation over a period of 11,100 years for MIS 1 (IMCCE, 2018).

However, in recent times, the cold air volume above 60N latitude has produced extreme weather events associated with an instability of the polar vortex - stable cold, dense air counter-rotating at northern latitudes - that is kept in check by the jet stream. The specific conditions that produce these events are not well understood due to the lack of a reliable theory of the earth's climate. At best, there are models (Lawrence et al., 2020) that attribute different physical mechanisms to these events. However, the recurrence of such events over an extended period can result in ice and snow accumulation that can change the earth's albedo, producing cooler climates because of gradual changes in the earth's heat engine. The monitoring of trends in the earth's albedo may provide a way of anticipating an eventual temperature descent into the next ice age.

It is essential to keep in mind that the above estimated MIS 1 termination is tentative. Nevertheless, based solely on the earth's celestial motions and the sun's rays, the Holocene termination is likely to happen as all other interglacial terminations over the last 800,000 years.

6. Summary

The partition model presented in this paper is a kinetic model based on the earth's celestial motions and the sun's rays. Its predictions reveal a recurring pattern over 800,000 years consistent in its interpretation of paleoclimate data and, in particular, interglacial terminations. The results regarding the future occurrence of an ice age are a simple extrapolation of the recurring pattern. If anything, it is a very conservative, albeit limited, approach to inferring when the next ice age will occur based solely on celestial mechanics and the sun's rays.

The model also provides additional insight into the roles of the precession index and obliquity contributions to the insolation described as a wave. In particular, the recurrence of interglacial and glacial periods over the last 800,000 years approximately correlates with the quasiperiodic behavior of PI wave packets. This correlation is reinforced by the quasiperiodic behavior of the O-Wave contribution to the insolation. In addition, all interglacial terminations involve constructive interference between the PI and O waves. Finally, interglacial durations approximately coincide with the number and duration of precession carrier wave cycles.

Based solely on celestial mechanical considerations and the sun's rays, the estimated Holocene termination will likely occur at 500 years from the present. The estimated duration of the glacial period that will follow this termination is about 36,000 years based upon the temporal duration of the precession index wave packet of Figure 12. After this period, there will likely be another increase in temperature, but the magnitude cannot be determined based solely on the partition model. To accomplish that would require a detailed climate model that consistently reproduces the features of the paleoclimate data over the last 800,000 years, which is far beyond the scope of this paper.

In terms of discrepancies, the comparison between the partition model predictions and EDC data indicates two interglacial inception timing issues. There are inception delays associated with MIS 18d and 13c (see Parrenin et al., 2007 for similar discrepancies between LR04 Benthic and EDC datasets); however, these may be due to physical effects related to the timing inferred from deep ice cores. Nevertheless, the considerable consistency of the PI and O waves predicted by the partition model over 800,000 years with data should motivate further examination of the timing inferred from EDC deep ice cores.

Finally, the consistency of the partition model predictions makes the search for a common physical mechanism within the earth's climate system that causes temperature descents into glacial periods more compelling. It is likely that a cumulative climate effect occurs over an extended period (the next 500 years) that eventually tips the earth into a persistent temperature descent concurrent with the decline in precession carrier wave maxima. This trend very likely impairs recovery until there is a return to increasing precession carrier wave maxima as Figure 12 indicates. Identifying the specific physical mechanism that causes this descent is far beyond the scope of this paper. Nevertheless, the potential expansion of the cold air volume at northern latitudes due to significant declines in insolation over the last 11,100 years should be investigated as a possible cause. Given recurring PI wave packets and their correlation with interglacial and glacial periods over the last 800,000 years, the possible catastrophic consequences to the future of civilization from another ice age should provide ample motivation to intensify scientific research in this vitally important area.

Funding

None

Guest-Editor: Martin T. Hovland; Reviewer: anonymous

Acknowledgments

I would like to acknowledge numerous exchanges with Professor William H. Smith of Washington University, St. Louis, concerning Milankovitch Theory. I would especially like to thank Dr. Patrick Frank and Patrice Poyet for reading the manuscript and making numerous helpful suggestions that measurably improved the clarity and presentation of the results. I am also indebted to Bruce Bauer, Data Manager, World Data Service for Paleoclimatology and NOAA National Centers for Environmental Information (NCEI) Climatic Science and Services Division – Paleoclimatology Boulder, CO for providing the relevant paleoclimate datasets. Finally, I would like to express my gratitude to Dr. Jacques Laskar for directing me to the wonderful computational tool he and his colleagues created, which enabled all the computations in this paper.

Appendix A

This section aims to derive equations (8) and (9) using light rays and vector analysis. The sun's light rays hit the earth with uniform intensity at angles relative to tangential planes over the earth's surface. However, there is a point on the earth where the rays are perpendicular to a tangential plane, the subsolar point. As the earth rotates, this point moves westward and north and south due to the earth's obliquity and orbit in a wavelike pattern completing an entire cycle over a year.

For an observer at a point on the earth looking vertically, there is a component of a solar ray parallel to the vertical and another tangential. The vertical component is of interest in determining the obliquity contribution to the insolation, while the tangential component is assumed lost. The key quantity to determine is the time-dependent zenith angle between an observer vector pointing vertically and the declination vector pointing from the earth's center to the subsolar point. The partition model assumes that the cosine of this angle times an overall constant determines the obliquity contribution to the insolation. Because the observer and subsolar point move relative to the sun, the mean daily insolation is the average of the cosine of the zenith angle over daylight hours.

The relevant angles and vectors defined with respect to the earth's body fixed rotating axes are represented in the following diagram,

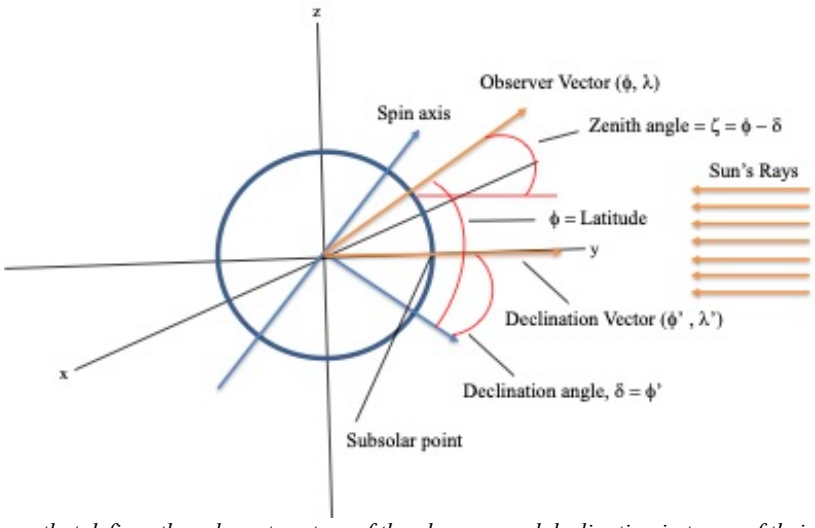

Figure 1A. A diagram that defines the relevant vectors of the observer and declination in terms of their latitudes and longitudes, (f , l) and (f'= d, l'), respectively defined with respect to rotating body fixed axes. The observer latitude and the declination angle, d, determine the zenith angle, z.

The observer unit vector in the rotating body-fixed frame is given by

$$\vec{V}_o = \cos(\emptyset)\cdot\cos(\lambda)\,\vec{i} + \sin(\phi)\cdot\cos(\lambda)\,\vec{j} + \sin(\lambda)\,\vec{k}, \qquad (1A)$$

and the declination unit vector is given by

$$\vec{V}_\delta = \cos(\emptyset')\cdot\cos(\lambda')\,\vec{i} + \sin(\phi')\cdot\cos(\lambda')\,\vec{j} + \sin(\lambda')\,\vec{k}, \qquad (2A)$$

where $\emptyset' = \delta$, the declination angle. The cosine of the zenith angle is simply the scalar product of equations (1A) and (2A) given by

$$\vec{V}_o \cdot \vec{V}_\delta = \cos(\zeta) = \sin(\phi) \cdot \sin(\delta) + \cos(\phi) \cdot \cos(\delta) \cdot \cos(h), \quad (3A)$$

where $h = \lambda' - \lambda$ is the hour angle, which for sunrise and sunset is determined by $cos(\zeta) = 0$ or

$$h_0 = cos^{-1}(-\tan(\emptyset) \cdot \tan(\delta)), \quad (4A)$$

which equals equation (9) for the summer solstice when $\delta = \theta$, the earth's obliquity angle.

For the partition model, we assume the obliquity contribution to the insolation during the summer solstice is of the form

$$B = G \cdot \big(sin(\phi) \cdot sin(\theta) + cos(\phi) \cdot cos(\theta) \cdot cos(h) \big) \quad (5A)$$

where G is an overall constant. The mean daily obliquity contribution to the mean daily insolation, $\bar{Q}$ of equation (2) is obtained by averaging equation (5A) over daylight hours given by

$$\bar{B} = \frac{G}{2 \cdot \pi} \cdot \int_{-h_0}^{h_0} (sin(\phi) \cdot sin(\theta) + \cos(\phi) \cdot cos(\theta) \cdot cos(h)) \; dh \quad (6A)$$

$$= \frac{G}{\pi} \cdot \big(h_0 \cdot \; sin(\phi) \cdot sin(\theta) + \cos(\phi) \cdot cos(\theta) \cdot sin(h_0) \big), \quad (7A)$$

from which equation (8) follows straightforwardly with h_0 determined by equation (4A) with $\delta = \theta$.

References

Berger, A., Loutre, M.F. and Crucifix M., The Earth's Climate in the Next Hundred Thousand Years (100 kyr), Surv. Geophys., Vol. 24, pp. 117–138, https://link.springer.com/article/10.1023/A:1023233702670, 2003.

Berger, A., Crucifix, M., Hodell, D.A, Mangili, C., McManus, J.F., Otto-Bliesner, B., Pol, K., Raynaud, D., Skinner, L.C., Tzedakis, P.C., Wolff, E.W., Yin, Q.Z., Abe-Ouchi, A., Barbante, C., Brovkin, V., Cacho, I., Capron, E., Ferretti, P., Ganopolski, A., Grimalt, J.O., Hönisch, B., Kawamura, K, Landais, A., Margari, V., Martrat, B., Masson-Delmotte, V., Mokeddem, Z., Parrenin, F., Prokopenko, A.A., Rashid, H., Schulz, M., and Vazquez Riveiros, N., Interglacials of the Last 800,000 Years, Rev. Geophys, Review Article, pp. 1-58, https://agupubs.onlinelibrary.wiley.com/doi/full/10.1002/2015RG000482, 2015.

Berger, W.H., Milankovitch Theory - Hits and Misses, Scripps Institution of Oceanography, Technical Report, pp. 1-35, https://escholarship.org/uc/item/95m6h5b9, 2012.

Gradstein, F., Ogg, J., and Smith, A., A Geologic Time Scale 2004, Cambridge University Press, Book, pp. 1-589, https://www.cambridge.org/core/books/geologic-time-scale-2004/ACED6139A9320FC9CA982E316FFF3E38, 2005.

Hays, J.D., Imbrie, John, and Shackleton, N.J., Variations in the Earth's Orbit: Pacemaker of the Ice Ages, Science, Vol. 194 (4270): pp. 1121–1132, https://www.science.org/doi/10.1126/science.194.4270.1121, 1976.

Huybers, P., Combined Obliquity and Precession Pacing of Late Pleistocene \Deglaciations, Nature, Vol. 480, pp. 229–232, https://www.nature.com/articles/nature10626, 2011.

Imbrie, J., Astronomical Theory of the Pleistocene Ice Ages, Icarus, Vol. 50 (2-3), pp. 408-422, https://www.sciencedirect.com/science/article/abs/pii/0019103582901324, 1982.

Imbrie, J., and Imbrie, K. P., Ice Ages: Solving the Mystery, Harvard University Press, Book, pp.1-224, https://www.hup.harvard.edu/catalog.php?isbn=9780674440753, 1986.

IMCCE, Virtual Observatory Solar System Portal, CNRS Observatory, Paris, http://vo.imcce.fr/insola/earth/online/earth/online/index.php, 2018. Numerical calculations in this paper make considerable use of data generated from this computational tool.

Jouzel, J., A Brief History of Ice Core Science over the Last 50 Years, Clim. Past, Vol. 9, pp. 2525-2547, https://cp.copernicus.org/articles/9/2525/2013/, 2013.

Laskar, J., Robutel, P., Joutel, F., Gastineau, M., Correia, A.C.M., and Levrard, B., A Long-Term Numerical Solution for the Insolation Quantities of the Earth, Astron. Astrophys., Vol. 428, pp. 261-285, https://www.aanda.org/articles/aa/full/2004/46/aa1335/aa1335.html, 2004.

Lawrence, Z.D., Perlwitz, J., Butler, A.H., Manney, G.L., Newman, P.A., Lee, S.H., and Nash, E.R., The Remarkably Strong Artic Stratospheric Polar Vortex of Winter 2020: Links to Record Breaking Arctic Oscillation and Ozone Loss, J. Geophys. Res.-Atmos., Vol. 125, pp. 1-21, https://doi.org/10.1029/2020JD034190, 2020.

Lisiecki, LE. and Raymo, M.E., A Pliocene-Pleistocene Stack of 57 Distributed Benthic $\delta^{18}O$ Records, AGU Paleoceanography and Paleoclimatology, Vol. 20 (PA1003), pp.1-17, https://agupubs.onlinelibrary.wiley.com/doi/epdf/10.1029/2004PA001071, 2005.

Lisiecki, L., Links between Eccentricity Forcing and the 100,000-Year Glacial Cycle, Nature Geoscience, Vol. 3, pp. 349–352, https://www.nature.com/articles/ngeo828, 2010.

Meyers S.R., Sageman B.B., and Pagani M., Resolving Milankovitch: Consideration of Signal and Noise, Am. J. Sci., Vol. 308 (6), pp. 770-786, https://www.ajsonline.org/content/308/6/770, 2008.

Milankovitch, M., Canon of Insolation and the Ice-Age Problem, Royal Serb. Acad., Spec. Publ., pp. 1-634, https://www.amazon.com/Insolation-Ice-Age-Problem-Milankovic-Milankovitch/dp/8617066199, 1998.

NCEI, EPICA Dome C – 800KYr Deuterium Data and Temperature Estimates, https://www.ncei.noaa.gov/access/paleo-search/study/6080, 2007.

Parrenin, F., Barnola, J.-M. , Beer, J., Blunier, T., Castellano, E., Chappellaz, J., Dreyfus, G., Fischer, H., Fujita, S., Jouzel, J., Kawamura, K, Lemieux-Dudon, B., Loulergue, L., Masson-Delmotte, V., Narcisi, B., Petit, J.-R., Raisbeck, G., Raynaud, D., Ruth, U., Schwander, J., Severi, M., Spahni, R., Steffensen, J.P., Svensson, A., Udisti, R., Waelbroeck, C., and Wolff, E.W., The EDC3 Chronology for the EPICA Dome C Ice Core, Clim. Past., Vol. 3, pp. 485-497, Figure 3, pp. 491, https://cp.copernicus.org/articles/3/485/2007/, 2007.

Roe, G., In defense of Milankovitch, Geophysical Research Letters, Vol. 33 (L24703), https://agupubs.onlinelibrary.wiley.com/doi/abs/10.1029/2006GL027817, pp. 1-5, 2006.

Rohling, E.J., Braun, K., Grant, K., Kucera, M., Roberts, A.P., Siddall, M, Trommer, G., Comparison between Holocene and Marine Isotope Stage -11 Sea Level Histories, Earth Planet. Sc. Letters, Vol. 291 (1-4), pp. 97–105, https://www.sciencedirect.com/science/article/abs/pii/S0012821X1000018X?via%3Dihub, 2010.

Vavrus, S.J., He, F., Kutzbach, J.E., Ruddiman, W.F., and Tzedakis, P.C., Nature: Scientific Reports, Vol. 8 (10213), pp. 1-12, https://www.nature.com/articles/s41598-018-28419-5, 2018.

Wunsch, C., Quantitative Estimate of the Milankovitch-Forced Contribution to Observed Quaternary Climate Change, Quaternary Sci, Rev., Vol. 23 (9-10), pp. 1001-1012, https://www.sciencedirect.com/science/article/abs/pii/S0277379104000575, 2004.

Zachos, J., Pagani, M., Sloan, L., Thomas, E., and Billups, K., Trends, Rhythms, and Aberrations in Global Climate 65Ma to Present, Science, Vol. 292(5517), pp. 686-693, https://www.science.org/doi/abs/10.1126/science.1059412, 2001.